Hydrogen Gas Gap Heat Switch operating in the 150 K to 400 K temperature range

Jorge Barreto[a,†], *Daniel Martins*[b,‡], *Moritz Castelo Branco*[b,c], *Joaquim Branco*[d], *António Pereira Gonçalves*[e], *T. Tirolien*[c], *Grégoire Bonfait*[a]

a) LIBPhys, Departamento de Física, Faculdade de Ciências e Tecnologia, Universidade NOVA de Lisboa, 2829-516 Caparica, Portugal

b) Active Space Technologies S.A., Parque Industrial de Taveiro, Lote 12, 3045-508 Coimbra, Portugal

c) European Space Agency, ESTEC, E0053A, 2200 AG Noordwijk, The Netherlands

d) CQE, Departamento de Engenharia e Ciências Nucleares, Instituto Superior Técnico, Universidade de Lisboa, 2695-066 Bobadela, Portugal

e) C2TN, Departamento de Engenharia e Ciências Nucleares, Instituto Superior Técnico, Universidade de Lisboa, 2695-066 Bobadela, Portugal

Corresponding Author

Jorge Barreto (e-mail: ja.barreto@campus.fct.unl.pt)

Present Addresses

† Omnidea Lda., Madan Parque Sul, Quinta da Torre, 2825-149 Caparica, Portugal

‡ ASML, De Run 6501, 5504 DR, Veldhoven, The Netherlands

Author Contributions

The manuscript was written through contributions of all authors. All authors have given approval to the final version of the manuscript.

Abstract

A prototype of a compact hydrogen gas gap heat switch (GGHS), built using the difference in the linear thermal expansion coefficients of copper and stainless steel, was designed to work in the temperature range of 150 K to 400 K. Using hydrogen, nitrogen and helium as working gas, a gap of 18 micrometers was measured. With hydrogen, an ON/OFF switching ratio higher than 100 was obtained at 150 K. A sorption pump was integrated to the GGHS and filled with the metal hydride $ZrMn_2$ to overcome the very low adsorption of hydrogen with activated carbon, material frequently used to manage the pressure in the gap. This solution allowed to reach both ON and OFF states by varying its temperature between 150 K and 300 K. The results obtained suggest that the proposed design allows for the development of tunable hydrogen heat switches while keeping the assembly very simple and sturdy.

Keywords

Gas Gap Heat Switch; Thermal expansion; Adsorption; Hydrogen; Metal Hydride

1. Introduction

The cryogenic heat switches are devices able to vary their thermal conductance by several orders of magnitude [1]–[3] and are fundamental pieces of some dynamic cryogenic systems. For instance, they have been used for a long time in adiabatic demagnetization refrigerators [4], [5], they would be useful to (de)couple redundant cryocoolers of the system to be cooled [6], they were also used in the Herschel satellite for thermal management of the ^{3}He cryocooler [7] and also attached to high enthalpy reservoirs for cryogenic thermal energy storage units [8], [9]. In these two last applications, Gas Gap Heat Switches (GGHS) were used [10] : they consist in two highly conducting blocks, usually copper, separated by a narrow gap. Introducing gas into this gap at a pressure corresponding to the viscous regime (mean free path λ << gap length Δ) leads to a highly conducting state (ON state), whereas pumping it down to the molecular regime (λ >> Δ) allows to drastically reduce the conduction between the two blocks. In a GGHS, this very low conducting state (OFF state) is usually limited by the thermal conductance of the mechanical support of the blocks, in parallel to the block-gap-block thermal path, that maintains the two blocks separated and aligned. The main benefits of a GGHS are that no mobile parts are needed, avoiding problems due to complicated mechanisms or material fatigue. Thanks to these advantages, they are very suitable for cryogenic systems in which long lifetimes are expected without any maintenance as in satellites, for instance.

In a GGHS, the shorter the gap, the greater the ON thermal conductance. In “usual” GGHS, gap lengths as small as 100 μm were obtained thanks to precise machining and somewhat delicate alignment procedures. Recently, a technique based on the difference in the linear thermal expansion coefficients (CTE) between the copper blocks and the stainless-steel (SS) mechanical support was used to obtain smaller gap lengths (down to 17 μm) without the need of such complicated procedures [11], [12]. Narrow GGHSs built using such technique were tested and showed good features in the 4 K to 300 K temperature range. However, one issue with this technique is that such narrow gaps were obtained through a soft-soldering procedure (≈ 180 °C) to join the stainless-steel support to the copper blocks, and the poor mechanical properties of this joint turns out this device not reliable if submitted to high vibration levels, as it occurs during the launch of a satellite, for instance.

In this paper, we describe a narrow GGHS to be integrated between a sorption compressor cell and a heat sink at a temperature of 150 K. As this sorption cell temperature has to vary in the 160 K to 400 K range, such a GGHS offers the ability to thermally (de)couple these two parts

and, thus, to optimize and control the dynamics of the heating and cooling phases of the sorption compressor [13].

After a brief description of how were calculated some basic features of such devices, we show the thermal characteristics of a narrow GGHS entirely assembled with a brazing process at 650°C, turning it much more structurally robust than the GGHSs previously built. Thermal conductance measurements were performed in the temperature range of 100 K to 300 K with hydrogen, nitrogen and helium gas to determine experimentally its gap length and its thermal conductance as a function of pressure to obtain the characteristic OFF to ON transition. For low temperature GGHS, the gas gap pressure management is usually obtained by using a small adsorption pump (referred as "sorption pump" on the following) filled with activated carbon: the very low pressure (OFF state) is reached by cooling it; whereas on heating, gas is desorbed and the ON state can be achieved. Unfortunately, a sorption pump for both helium and hydrogen (the highest conducting gases, so, the most suitable for GGHS) is limited to the low temperature range, typically below 20 K for helium and 40 K for hydrogen, very far from our 150 K heat sink temperature. As already experienced [7, 8] or proposed [16], another way to pump hydrogen gas down to suitable pressures to achieve the switching action of a GGHS (typically below 10^{-1} mbar) is H_2 adsorption using adequate intermetallic materials. In the second part of this article, the features of a GGHS integrating a sorption pump filled with the intermetallic compound ZrMn2 are described and compared to what was expected in the 150 K to 300 K temperature range.

2. Narrow GGHS and Experimental Set-up

2.1 Narrow GGHS building

The ON↔OFF switching mechanism of a dilation GGHS is based on the same principle of an usual GGHS, the difference being that the gap is obtained thanks to the thermal expansion coefficient (CTE) difference between the material used for the supporting shell (stainless steel) and the two conducting blocks (copper) [12]. In the devices presented in this paper, these two copper blocks are cylindrical and are maintained face-to-face thanks to a Stainless-Steel Supporting Shell (SSSS), consisting in a thin wall tube (Figure 1a). The SSSS length is such that it allows physical contact between the copper blocks after mounting: the gap between the copper blocks is then null before brazing and must be kept as short as possible, ideally null, during the brazing process. After brazing and during cooling, due to the higher CTE of copper in respect to stainless steel, the total length of the copper blocks becomes shorter in comparison

with that of the SSSS and a gap is formed (Figure 1b). One advantage of such technique is that it requires a much simpler manufacturing and assembly procedure, since the gap is "naturally" obtained and the delicate machining and alignment procedures to prevent contact between the copper pieces in usual GGHS are avoided.

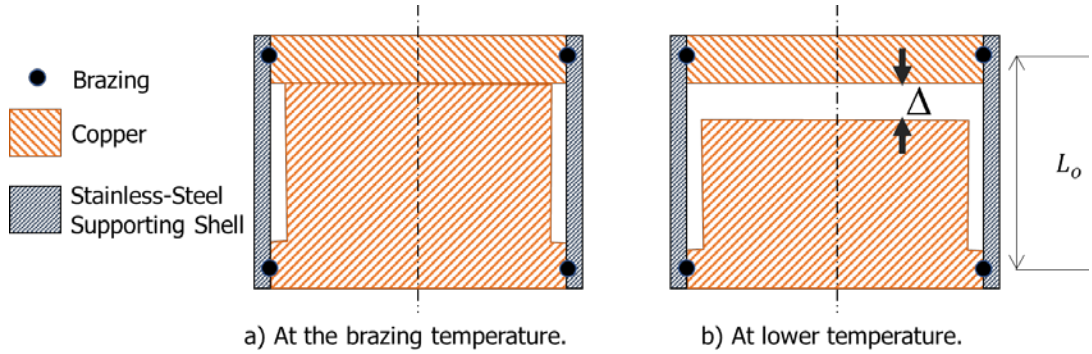

Figure 1: Cross-sectional schematic view of a dilation GGHS at the brazing temperature (left) with the copper blocks in contact, and after brazing and during cooling (right) where a gap, Δ, naturally appears due to the difference in the CTE of copper and stainless-steel.

Such narrow GGHSs were built and tested between 20 K and room temperature with relative success: below 80 K, where CTE becomes negligible, a gap length of 17 μm was obtained, significantly longer than the 8 μm previously calculated [11], [12]. Due to the gap formation technique, the soldering/brazing temperature, T_0, should be as low as possible to minimize the gap appearing due to the device cooling from T_0 down to room temperature. In [11], a common soft-soldering was used with a melting point of 180°C to reduce this effect. However, at that time, such soldering procedure was performed on a workbench and the external surface of the SSSS was exposed to air and naturally cooled by convection, so, remaining over a significant length at a temperature lower than that of the copper blocks: after soldering and during cooldown, the SSSS contracted less than expected, explaining why the gap length was found significantly longer than calculated (6 μm at 80K), assuming a homogeneous temperature during soldering. Despite this issue, such device was tested with helium and nitrogen gas and its thermal features found in good agreement with developed thermal models. However, for some applications, as its integration in a satellite thermal bus, such soft soldering cord is not mechanically strong enough to withstand the high levels of vibration. Consequently, a new narrow GGHS was built using a silver alloy for brazing ($T_0 = 650$°C) that turns out this mechanical joint sturdier. Moreover, to minimize the gap, special care was taken to avoid temperature inhomogeneity during brazing, as occurred previously.

2.2. Gap length calculation

Three slightly different gas gap heat switches were built (GGHS #1, #2 and #3). Their main parts (Figure 2) are cylindrical and their geometrical and thermal characteristics shown in Table 1. The cylindrical copper blocks were machined from "normal" copper (RRR between 50 and 100). The supporting shells were obtained from a commercial tube (GGHS #1) or machined by us (GGHS #2 and #3). To avoid long thermal response times during the characterization tests, one of the copper blocks (hot side) was designed as short as possible to reduce its mass and, therefore, the length to be considered for the linear thermal expansion and for the thermal conductance calculus is mainly from the cold block one. The GGHS #2, shown in Figure 2, includes a small sorption pump connected by a ≈20 mm length stainless steel capillary (further details in Section 4).

Contrarily to the procedure used in the previous versions of these type of GGHS [11], to avoid a significant temperature difference between the copper blocks and the SSSS during brazing, the whole device was heated up to the brazing paste melting point temperature ($T_o = 650$°C) in a temperature-controlled oven filled with nitrogen gas.

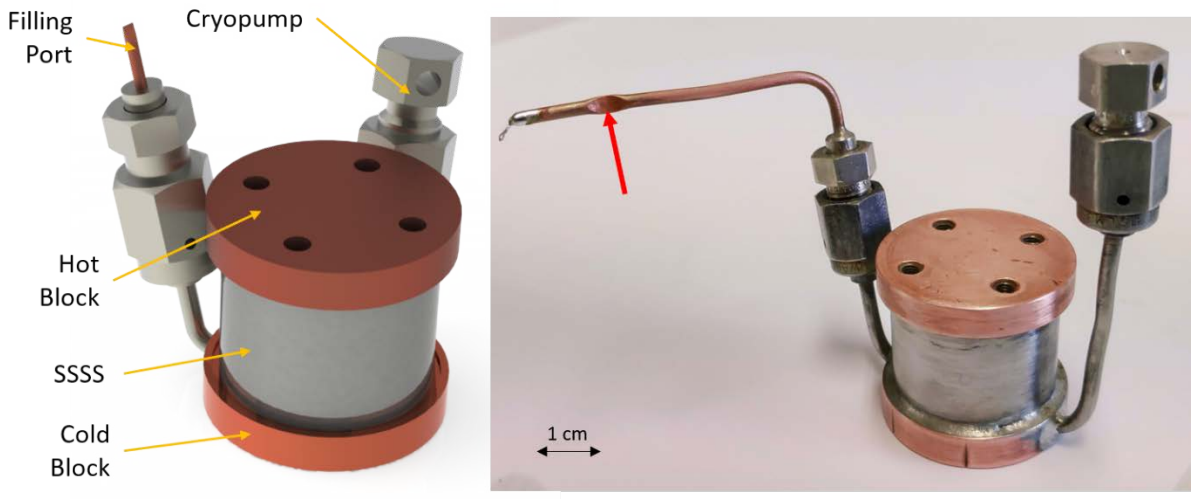

Figure 2: Dilation GGHS #2 rendered image (left side) and as built (right side). The red arrow points to the location of the "pinch-off" sealing. This sealed switch is the one used to obtain the results "Sealed Desorption/Absorption" displayed in Figure 8.

Considering the GGHS geometry, if the two copper blocks are in contact at T_o, while considering the entire length of the SSSS also at the same temperature during this procedure, the gap length Δ(T) at a temperature *T* can be calculated as follows:

$$\Delta(\mathrm{T}) = L_o \int_{T_0}^{T} \left(\alpha_{Cu}(T) - \alpha_{SS}(T)\right) dT \qquad \textbf{Equation 1}$$

where L_o is the length of the SSSS at T_0, α_{Cu} and α_{SS} are the CTE of copper and stainless steel, respectively.

Table 1: GGHS geometrical characteristics and expected thermal performance at 150 K with hydrogen as the exchange gas.

GGHS number / **Feature**	**#1**	**#2**	**#3**
GGHS total length	24.8 mm	29 mm	34 mm
Inner copper block length ($L_{Cu} = L_o$)	17.0 mm	17.0 mm	17.0 mm
Inner copper block diameter	17.5 mm	24.8 mm	25.0 mm
Face to face area (A)	2.41 cm^2	4.83 cm^2	4.91 cm^2
Mass	64.0 g	167.4 g	160.1 g
SSSS external diameter	18.92 mm	26.26 mm	26.27 mm
SSSS thickness	110 µm	130 µm	114 µm
SSSS length (L_{SSSS})	18.8 mm	18.8 mm	18.8 mm
α_{Cu} (300 K) [17]	16.6×10^{-6}		
α_{SS} (300 K) [17]	15.4×10^{-6}		
Gap Δ at 150 K	≈ 15 µm		
Gas-gap conductance (H_2)	1.60 W/K	3.21 W/K	3.27 W/K
Cu block conductance	5.23 W/K	10.5 W/K	10.7 W/ K
K-ON	1.23 W/K	2.46 W/K	2.50 W/K
K-OFF (SSSS)	3.9 mW/K	6.3 mW/K	5.6 mW/K
ON/OFF ratio	3.2×10^2	3.9×10^2	4.5×10^2

The linear expansion coefficients obtained from various databases (NIST [17], Matweb [18], Touloukian [19]) present small differences and the gap length depending on the difference of two very similar CTE coefficients (Table 1), these discrepancies can lead to quite different gap lengths: for instance, a relative uncertainty of 1% on each CTE leads to a gap uncertainty of 40%. So, in such conditions, a precise $\Delta(\mathrm{T})$ calculation becomes quite challenging. Then, to obtain a rough approximation of the gap values, we decided to calculate it by considering the NIST values for copper and SS316 in the temperature range of 4 K to 300 K and keeping constant the differential CTE from room temperature up to the 650°C. This calculation leads to the $\Delta(\mathrm{T})$ displayed in Figure 3 ($\Delta_o = 0$ line). The experimental gap determinations, obtained with various gases as explained in the following section, are presented on the same figure, and show that this crude extrapolation may not be so far from reality. In any case, below 90 K, the

calculated gap length is almost constant, reflecting that, as for most metals, the CTE of copper and SS become residual in this temperature range. In the range 100 K to 300 K, the NIST data lead to a linear behaviour of the gap length variation with temperature (nearly constant α for both metals in this range). Usually, for temperatures higher than 300 K, the CTE tends to increase. Then, extrapolating this linear behaviour for higher temperatures would mean, for instance, that this increase is equal for both materials. Using this rough extrapolation, the gap obtained at 150 K would be about 15.2 µm (considering $\Delta = 0$ at 650°C). If for any mechanical reason (e.g., high roughness, solid impurities between the two blocks, parallelism defect of the copper blocks) the gap at the brazing temperature $\Delta_o = \Delta(T_0)$ is not zero, the final gap will be obtained by adding a non-null Δ_o to the calculated values displayed in Figure 3 (Δ_o=0 µm line).

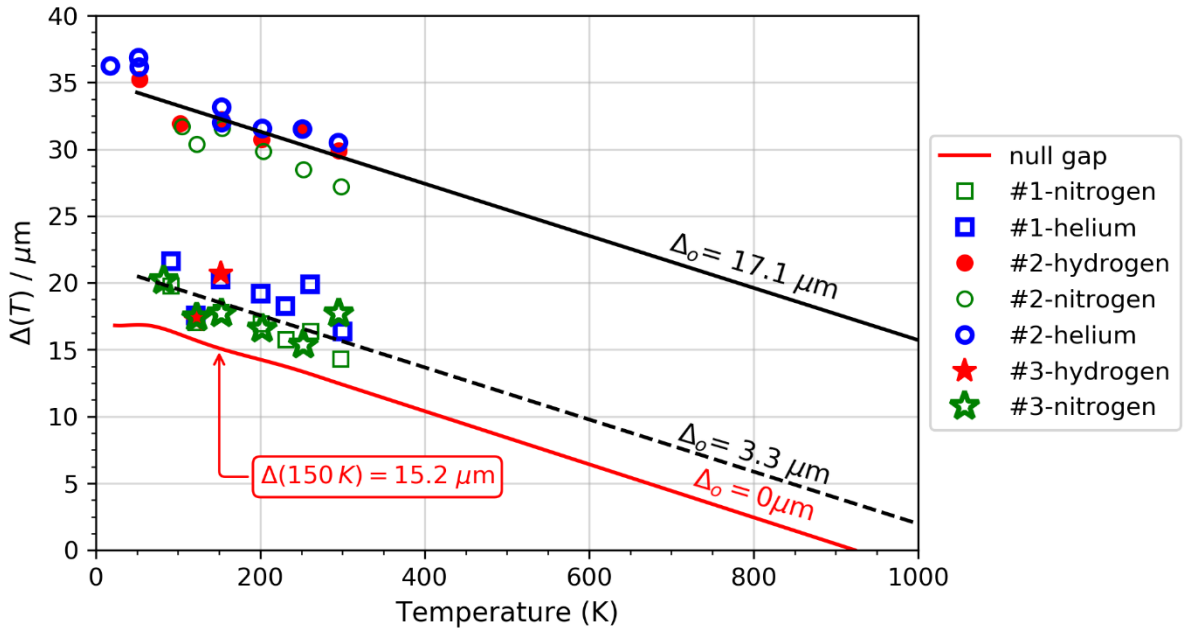

Figure 3: Gap length $\Delta(T)$ as a function of temperature considering L_o =17 mm and various values for the gap length Δ_o at T_0. The symbols represent the experimental gap determination for GGHS#1-3 using various gases as explained in Section 2.3.

2.3 Experimental Setup and Thermal Conductance Determination

The experimental setup is very similar to those used in previous GGHS characterizations [10], [11]. The long copper block (cold block) is thermally coupled to the cold finger of a 4 K two stage Gifford-McMahon cryocooler and three previously calibrated thermometers are thermalized to the copper block and to the sorption pump (if any); one small heater (1.2 kΩ electronic resistor) is attached to the shorter copper block (hot block) to create a heat flux across the switch; for GGHS #2, another resistor was placed on the sorption pump to control its temperature. A short stainless-steel tube capillary is brazed to the cold block and ends by a

female tube fitting (Fig. 2). For GGHS#1 and #3, a 1-meter long SS capillary, ended by the male part, links the inner part of the switch to a room temperature gas manifold for gas management and pressure measurements. For GGHS #2, as depicted in Figure 2, a small portion of annealed copper capillary is placed between the long SS capillary and the male tube fitting: pinching this portion will allow to permanently seal the device (Cf. Section 4.2) and turn it easily autonomous. To precisely measure the thermal conductance, the cold block temperature, T_{CB}, was kept constant and various heat loads, $\dot{Q}$, were applied on the hot block (T_{HB}) while keeping, in most cases, $\Delta T = T_{HB} - T_{CB}$ below ≈10 K. At equilibrium, the corresponding temperature T_{HB} was measured and the thermal conductance K is then calculated as the slope of $d\dot{Q}/dT_{HB}$. Such method allows to minimize errors due to some parasitical heat loads or small calibration imperfections. However, this method imposes equilibrium states that can be very long to be reached if the thermal conductance decreases. Then, to speed up the conductance measurements as a function of the sorption pump temperature, T_{sorb}, a dynamic method, similar to that used for specific heat determination [8], [20], was used and lead to the results of Figure 8. In such a method, the hot block temperature is maintained slowly drifting, keeping ΔT around 10 K, by applying some external heating for instance, and its temperature variation $T_{HB}(t)$ is recorded. By (numerical) time derivative, $\dot{T}_{HB}$ (=dT_{HB}/dt) is calculated and the thermal conductance of the GGHS can be obtained as:

$$K(\bar{T})(T_{HB} - T_{CB}) = \dot{Q} - C\dot{T}_{HB} \qquad \textbf{Equation 2}$$

where $K(\bar{T})$ is the mean conductance between T_{HB} and T_{CB}, $\dot{Q}$ is the heat input applied to the hot block (considered much higher than the parasitical heat load) and C is the hot block heat capacity, calculated using its mass (≈ 33 g) and the NIST data for copper [17]. Simultaneously, by also varying (slowly) the sorption pump temperature T_0 between ≈150 K and ≈400 K (Section 4) and using Equation 2, the measurement of the GGHS conductance during the OFF↔ON transition is obtained in only one run (typically one day). Though this method is not as precise as that using static conditions, it allows a much faster characterization since the long stabilization times of the hot block temperature and of the sorption pump are not required. From previous measurements [11], the contribution of the thermometer, the heater and other small pieces to the hot block heat capacity were estimated to be equivalent to ≈3 g of copper, value found coherent after comparing the dynamic results to the static ones.

3. Experimental Results (without sorption pump)

3.1 ON Thermal Conductance and Gap Length Determination

The ON state conductance of the GGHS, K_{ON}, is obtained when the gas in the gap is in the viscous regime, characterized by a thermal conductivity independent of the pressure. To confirm if such regime is achieved, it is then experimentally verified that two K_{ON} determinations at different pressures give the same results. Figure 4 shows the ON thermal conductance of the GGHS #2 in this regime for three different gases. The pressure in the heat-switch used for these measurements was kept constant and measured at room temperature (450 mbar, 520 mbar, 620 mbar for H_2, He and N_2 respectively).

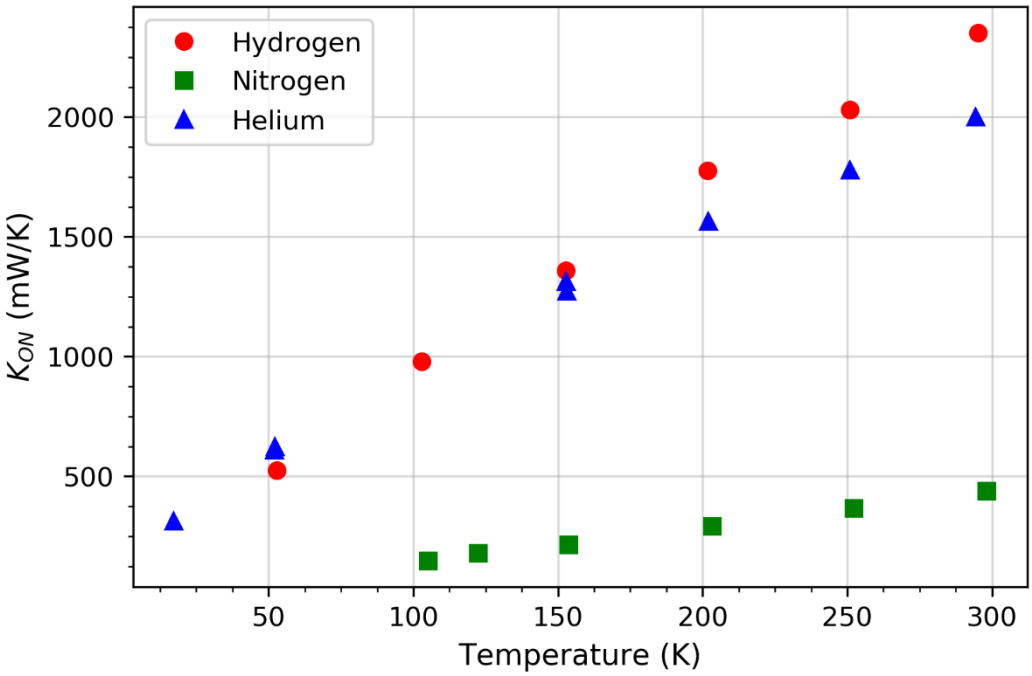

Figure 4: Experimental thermal conductance K_{ON} of GGHS #2 using various exchange gases. Note that, for T>150 K, the highest conductance is obtained with the GGHS filled with hydrogen gas instead of helium: this fact reflects the cross-over of the thermal conductivity of these two gases around this temperature.

To obtain the gap length from these results, the ON conductance K_{ON}must be separated into two major contributions:

- K_{Δ}, arising from the gas thermal conduction through the gap.
- K_{Cu}, coming from the conduction along the copper block, which can be calculated as $k_{Cu} \times A/L_{Cu}$ (k_{Cu}: copper thermal conductivity [17], A: face-to-face area of the copper blocks).

Considering these two thermal path in series, K_Δ can be calculated as $K_\Delta = K_{Cu} \times K_{ON}/(K_{Cu} - K_{ON})$ and, in the viscous regime, the gap length is given by $\Delta = k_{gas} \times A/K_\Delta$ (k_{gas} : gas thermal conductivity [21]). $\Delta(T)$ was calculated from the $K_{ON}(T)$ experimental values of GGHS#1-3 and these results are displayed in Figure 3 to be compared with the expected results ($\Delta_0 = 0$ line). In the same chart, are also plotted two other lines ($\Delta_o = 3.3$ µm, $\Delta_o = 17.1$ µm) representing $\Delta(T)$ calculated from the differential CTE, as previously described, but only differing by a vertical shift Δ_o which corresponds to a non-zero gap value at the brazing temperature T_0. These Δ_o values were adjusted to describe the experimental results for the gap length. Some remarks are noteworthy:

- Within the experimental errors, the experimental gas gap determination is independent of the exchange gas, which validates our data analysis.
- The results for two different GHHS (#1-squared and #3-stars) are identical and not far from the $\Delta_0 = 0$ prediction. This could indicate that Δ_0 is effectively null for these two heat switches, but that the considered extrapolation for the 300 K to 900 K temperature range of the CTE coefficients leading to a linear dependence of $\Delta(T)$ in this range is not valid. For instance, the obtained value of Δ_0 could be explained by an increase of the differential CTE, $\left(\alpha_{Cu}(T) - \alpha_{SS}(T)\right)$, in the extrapolated temperature range. Let us mention that the relatively small values of Δ_0 (≈3 µm) could also be compatible with some mechanical imperfections that may occur during the manufacture or assembly of the parts, which would prevent a full contact between the two copper surfaces when the brazing procedure begins. The fact that Δ_0 is similar for the two devices would be a coincidence.
- On the other hand, the data obtained for the GGHS#2 (circles) corresponds to a large shift ($\Delta_0 \approx 17$ µm) which, most likely, can be attributed to some troubles that occurred during its manufacture and/or brazing, leading to a real large gap at the brazing temperature.

3.2 OFF Thermal Conductance

To obtain the lowest conductance state (OFF state), the pressure between the two blocks must be low enough to reach the ballistic (or molecular, or Knudsen) regime in which the conduction through the gas becomes linear with pressure. In this regime, at very low pressure, the thermal conductance through the gas-gap becomes much lower than that through the SSSS. Then, in this condition, the heat load $\dot{Q}(T_{HB}, T_{CB})$ through the GGHS is given by:

$$\dot{Q}(T_{HB}, T_{CB}) = \frac{A_{SSSS}}{L_{SSSS}} \int_{T_{CB}}^{T_{HB}} k_{ss}(T) dT \qquad \textbf{Equation 3}$$

where A_{SSSS} represents the cross-sectional surface of the SSSS and k_{SS} is the thermal conductivity of the stainless steel [17]. The results of this equation for GGHS#2 are displayed in Figure 5 (solid line, "model SSSS") as a function of $\Delta T = T_{HB} - T_{CB}$, with $T_{CB} = 150$ K.

In the same figure are also displayed the corresponding experimental data of $\dot{Q}(\Delta T)$ for the GGHS#2 in the OFF state obtained by two ways. The first one (solid circle symbols) is obtained on before the sorption pump functionalization (i.e., no absorption material inside): the inner volume of the GGHS was connected directly to the vacuum (< 10^{-4} mbar) existing in the vacuum jacket of the cryocooler. This configuration leads to a very low pressure in the gap and thus ensures that the OFF state is reached. On the other hand, the squared symbols correspond to data obtained with the same GGHS after the installation of the operational sorption pump (right side of Figure 2) filled with an intermetallic material and sealed by pinching off the copper capillary with a charge of gas H_2 that allows to reach the ON state if heated (further details in Section 4). For these measurements, the sorption pump temperature is maintained at 150 K, temperature at which the intermetallic compound is expected to reduce drastically the H_2 pressure. These two sets of data show that either with the device externally pumped or sealed with the metal hydride, the OFF-state performance is similar in both scenarios, showing that the sorption pump can ensure the OFF state. For $\Delta T \leq 60$ K (dashed blue line), both results agree with the model, leading to an OFF conductance of approximately ≈ 8.4 mW/K. For higher ΔT, the discrepancy between the data and the model (Equation 3) can be explained considering the radiative heat transfer between the copper blocks. For instance, the simple Stefan-Boltzmann equation, $\dot{Q} = \varepsilon\sigma A(T_{HB}^4 - T_{CB}^4)$, using an emissivity ε= 0.35 and an exchange surface A equal to the cross-sectional area of the copper blocks, leads to the red dot-dashed line in very good agreement with experimental data. Similar agreements were found for GGHS #1 and #3. Let us note that a lower OFF conductance could be obtained by using a titanium alloy for the supporting shell (over a large temperature range, the thermal conductivity of stainless steel is about twice that of titanium). However, the absorption of H_2 in titanium can lead to its embrittlement and some precautions to prevent this effect must be taken. Moreover, the titanium thermal expansion coefficient is almost 4 times smaller than that of stainless steel or copper [17, 18] leading to a differential expansion much larger: a crude estimation using Equation 4 would lead to a gap larger than 100 µm at 150 K for the same brazing temperature T_o.

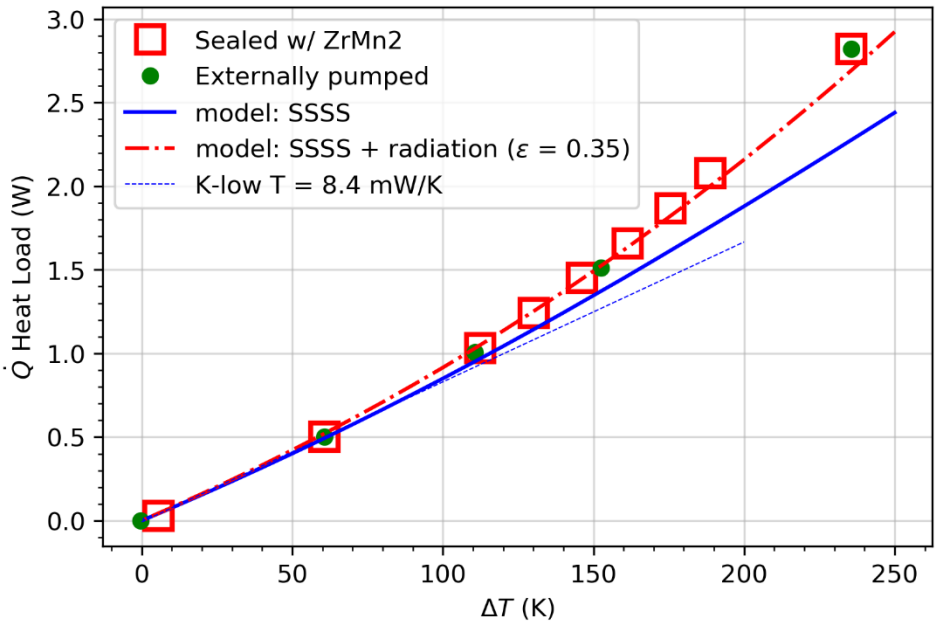

Figure 5: Heat load through GGHS#2 versus $\Delta T = T_{HB} - T_{CB}$ in the OFF state, $T_{CB} = 150$ K.

3.3 ON↔OFF Transition

In general, in such GGHS, the ON↔OFF transition is controlled by varying the pressure, *P*, in the gap thanks to heating/cooling of a sorption pump containing a material able to desorb/adsorb the working gas. The correct operation of this actuator is then dependent of the adequate adsorptive capacities of the pair gas/adsorbent in the targeted operating temperature range. That is why the variation of the GGHS #2 thermal conductance $K(P)$ in respect to the working gas pressure has been firstly carefully measured without an adsorbing material in the sorption pump. This conductance was measured for $T_{CB} = 150$ K in the pressure range 4×10^{-3} mbar to 800 mbar for both H_2 and N_2, the results (symbols) are displayed in Figure 6. The experimental results are also fitted to a previously developed thermal model where the gas gap conductance in the intermediate regime is calculated by considering a contribution of both ballistic and viscous conduction regimes [22]. For the ballistic regime, the accommodation coefficients, which are dependent of the gas and of the surface material, were obtained by fitting the experimental results and were found to be 0.38 and 0.83 for hydrogen and nitrogen gas, respectively, in line with previous works [16]. The results of this model for the thermal conductance are displayed as solid lines in Figure 6.

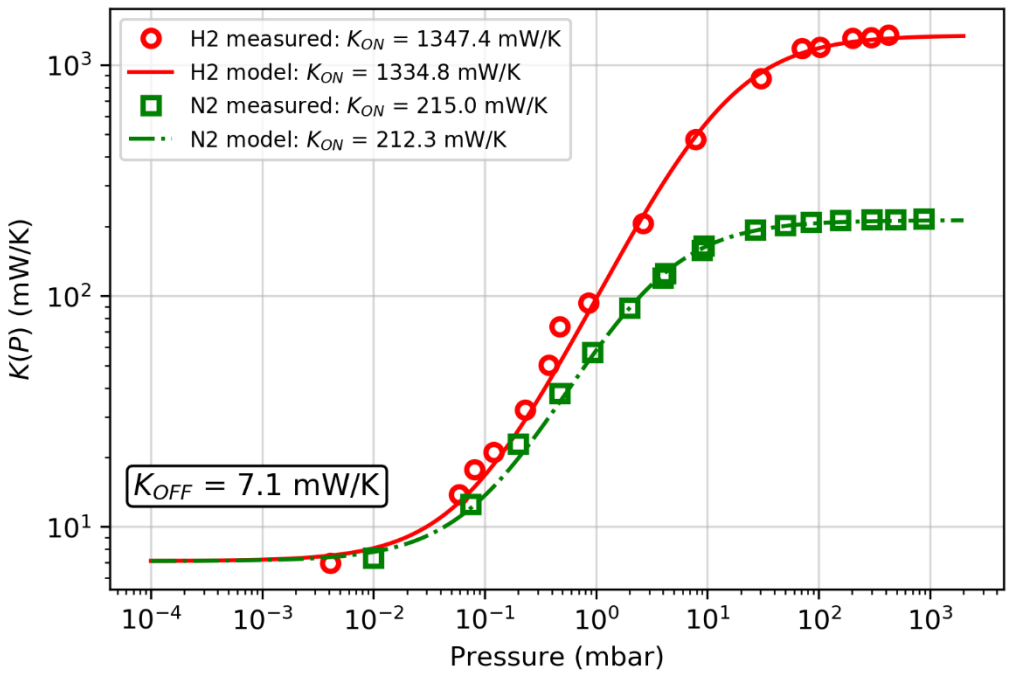

Figure 6: Measured thermal conductance $K(P)$ as a function of pressure for GGHS #2 using hydrogen (circle) and nitrogen (square) as exchange gas. The solid lines correspond to the fit of the conductance using an accommodation coefficient of 0.38 for hydrogen and 0.83 for nitrogen.

As expected, in the high-pressure regime, the GGHS conductance (~1350 mW/K for H_2 and ~215 mW/K for N_2) does not depend on pressure and is the same as previously obtained in the viscous regime measurement at 150 K (Figure 4). On the other hand, at low pressure, the gas gap conductance becomes very low and the SSSS ensures the main thermal path leading to both pressure and gas independent OFF constant value (≈7.1 mW/K). Between these two extreme states, the smooth transition ON↔OFF is very well described by our model for both H_2 and N_2 gas. Considering these results, the sorption pump adsorbent material required to obtain the ON↔OFF switching action must be able to vary the gap pressure by four orders of magnitude: from ≈100 mbar at high temperature to ≈ 0.01 mbar for T_{sorb} =150 K.

4. GGHS driven by a metal hydride sorption pump

4.1 ZrMn2 Preparation and Characterization

As previously explained, the ON thermal conductance is strongly dependent on the thermal conductivity of the working gas. From this point of view, helium and hydrogen are the best choices. However, both gases require low temperatures to be sufficiently adsorbed by a sorption

pump filled with activated charcoal, typically 20 K for helium [8] and 50 K for hydrogen [23], [24] temperatures not in accordance with the present requirements (base temperature at 150 K). Nevertheless, in the case of hydrogen another possibility is to use the ability to be reversely adsorbed and desorbed in metal hydrides, which can occur at a temperature a priori compatible with our goal [16]. Let us note that intermetallic hydrides have already been used in the space scientific mission Planck, from ESA, to build a hydrogen sorption compressor [25] and for hydrogen storage in a thermal energy storage unit working at 15 K [26]. In the present application, to avoid a sorption pump working at high temperatures, the hydrogen desorption leading to the ON state should occur up to 400 K, whereas adsorption, leading to the OFF state, needs an equilibrium pressure of 0.01 mbar (Figure 6) for $T \geq 150$ K. Despite the extensive investigation performed on materials for H_2 absorption, few data are available in this temperature and pressure range; taking into account these criteria, the intermetallic $ZrMn_2H_2$ (hydrogenate form) seems an appropriate choice (Figure 7 solid lines) [16], [27].

The $ZrMn_2$ intermetallic material was prepared by arc melting a mixture of 99.9% pure metals under argon atmosphere. Due to the high vapor pressure of manganese, and to compensate their possible losses by evaporation during melting, a 10-20% excess of this metal was considered. After each melting procedure, the sample was turned out and re-melted again for three times to obtain a homogeneous material. Powder X-ray diffraction patterns were collected at room temperature from fine powdering the samples and using Cu Kα radiation with a 2θ-step size of 0.02º from 10º to 70º. The analysis of the diffractograms indicate that the samples are mainly constituted by $ZrMn_2$ (~95% vol.) with minor amounts of Mn (~5% vol.). Following the process described in [28], [29], the activation of $ZrMn_2$ under H_2 was made at 50 bar under pure hydrogen on a stainless steel (316) plug & flow type reactor (continuous type reactor). A pressure controller to manage the reactor internal pressure and a mass flow controller to adjust the hydrogen flow (50 cm^3/min) were used. The following procedure was employed:

i) Reactor purge at atmospheric pressure with hydrogen (50 cm^3/min; 30 min).
ii) Raise of pressure until 50 bar.
iii) Raise of temperature until 600 ºC.
iv) At 600 ºC for 1h.
v) Decrease of temperature until room temperature, maintaining the pressure at 50 bar.
vi) Release of pressure until atmospheric pressure.

This treatment was repeated three times. A nitrogen-filled glove box (O_2 and H_2O content < 3 ppm) was used to handle the activated samples.

A rudimentary experimental setup was built to check if the pressure-temperature equilibrium curve of this material was compatible with our requirements in the 150 K to 400 K range. The setup consisted in a 0.5 cm^3 SS cell filled with ≈ 2 g of $ZrMn_2$ and connected to a ≈ 26 cm^3 volume at room temperature. A thermocouple type K and a heating resistor was thermally coupled to this cell to manage its temperature. This cell is slowly introduced in a partially filled liquid nitrogen Dewar or heated in this N_2 atmosphere to obtain a characterization over the temperature range of interest. The equilibrium pressure is measured by two different pressure transducers (0-13 mbar, capacitance sensor and 0-20 bar, piezoresistive sensor).

Figure 7 shows the obtained results for two different batches compared to the literature data [16], [27]. Despite their rough character, these measurements showed that the equilibrium pressure $P(T)$ seems significantly higher compared to the literature, further studies should be carried out to verify these results. Let us note that these measurements were performed with a [H]/[Mn] (total number of hydrogen atoms / total number of manganese atoms) ratio of about 60% to avoid saturation of ZrMn2 by hydrogen. Some measurements performed in the 300 K to 400 K temperature range (not shown) indicate that, at constant temperature, the equilibrium pressure increases as the [H]/[Mn] ratio increases; once again, a more rigorous characterization is needed to determine if such increase is intrinsic to this compound or if monophasic samples would lead to an independent equilibrium pressure with hydrogenation, as far saturation is not reached, as it is the case, for instance, for a $LaNi_5$ ($LaNi_5H_5$) compound [30]. However, even with this equilibrium pressure being higher than expected, this material seems to fulfill our needs: 0.01 mbar is reached at a temperature of 140 K and 100 mbar around 290 K. So, it was decided to use this material for the hydrogen sorption pump.

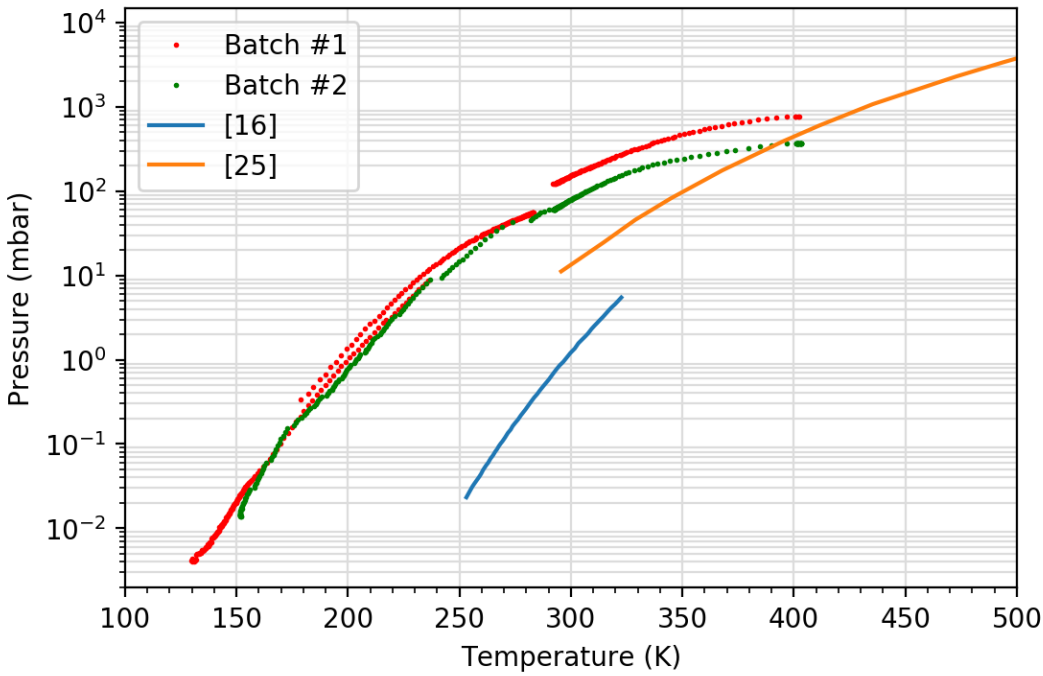

Figure 7: Equilibrium pressure-temperature curve of two synthetized batches of the metal hydride $ZrMn_2H_x$ and comparison with literature.

4.2 Results with ZrMn2 sorption pump

As depicted in Figure 2, a small sorption pump was coupled through a short SS capillary (≈ 30 mm) to the cold block of GGHS #2. This sorption pump was thermalized to the same part by a copper thermal link to speed up its cooling. Its volume was around 0.08 cm^3 and charged with 260 mg of ZrMn2 (batch #2) in an argon-filled glove box. For the first characterizations, the small copper portion was not pinched and the GGHS was connected to the room temperature gas manifold to charge it with hydrogen gas. Three different hydrogen fillings were tested using low [H]/[Mn] ratio to turn more favorable the OFF state at 150 K.

The full GGHS functionality was tested by measuring the ON↔OFF transition curve by varying the sorption pump temperature. The conductance results, obtained with the dynamic method (Section 2.3), are displayed in Figure 8 for these three hydrogen fillings. The "S-shaped" curves, similar to those of Figure 6, indicate that, as expected, the H_2 pressure in the gap increases with the sorption pump temperature. At $T \approx 150$ K, the GGHS reaches the OFF-state value (≈8 mW/K) for the 1.1 % and 5.4 % filling whereas, for the 16% filling, it seems not fully reached. In the transition regime, at a given temperature, the heat switch conductance clearly increases with the H_2 quantity in the system, confirming that the $P-T$ equilibrium curve of this $ZrMn_2$ material is then dependent of the adsorbed H2 quantity. For instance, at

$T = 250$ K and combining the data from Figure 7 and Figure 8, it can be deduced that the pressure in the heat switch is approximately 0.65 mbar, 1.1 mbar and 3.5 mbar for the 1.1%, 5.4% and 16% filling ratios, respectively. As already mentioned for the GGHS using activated charcoal [10], [22], such a characteristic can be useful as it allows to tune the ON and OFF switching temperatures in a certain range just by varying the H_2 quantity in the system.

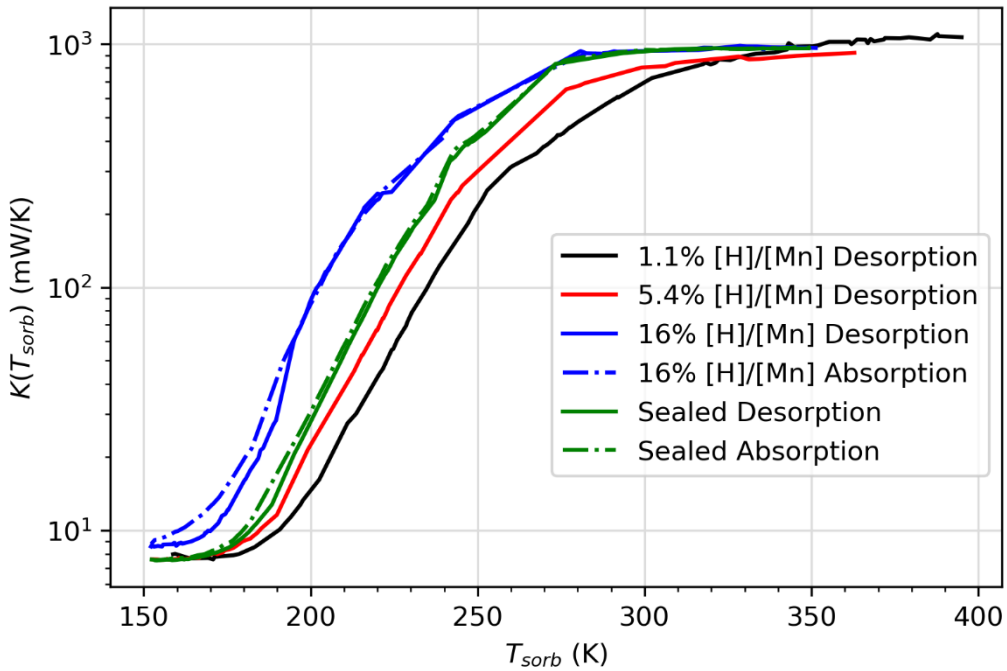

Figure 8: Measured thermal conductance of the GGHS #2 as a function of the hydrogen sorption pump temperature for different filling [H]/[Mn] ratios.

Regarding the ON state (sorption pump at high temperature), the thermal conductance reaches a constant value (≈ 1000 mW/K) for all H_2 fillings, as expected for the viscous conduction regime. However, note that this value is slightly less than the value obtained without sorption pump (≈1350 mW/K, referring to Figure 6). This fact could be explained by supposing that the gas desorbed from the $ZrMn_2$ on heating it up to 330 K is not enough to reach the pressure needed to achieve a full viscous conduction. Comparing with the results displayed in Figure 6, this value of 1000 mW/K would correspond to a gas-gap pressure of 30 mbar whatever the H_2 filling ratio. This pressure value is rather small compared to the obtained $P - T$ equilibrium curve (Figure 7), where this pressure is reached at ≈ 250 K. We looked without success for some experimental errors that could explain this discrepancy between these two ON state conductance values. Additional work is needed to understand if this issue is due to $ZrMn_2$ absorption characteristics or to another unknown reason.

A significant hysteresis during a desorption-absorption cycle would further complicate the use of such GGHS, then its thermal conductance was determined in both heating and cooling of the sorption pump using, approximately, the same heating/cooling rate (±12 K/hour). Figure 8 displays these results for the 16% filling in dot-dashed and solid lines for absorption (cooling) and desorption (heating), respectively. Within the experimental error, no significant hysteresis was detected, and a similar conclusion was obtained for the other two filling ratios.

In the framework of the future use of this device, we were more interested in avoiding high temperatures in the sorption pump to reach the ON state rather than a very low OFF conductance, then we decided to seal the GGHS with a H_2 quantity corresponding to the 16% filling ratio. After this sealing, the new ON↔OFF curve was measured (green lines of Figure 8): its extreme conductance values of both ON and OFF conductance values remained like those measured before and no significant hysteresis was detected. The main difference between the 16% curve is that the S-shaped curve became significantly narrower in respect to the temperature axis: the intermediate region between +10% of the OFF value and -10% of the ON value was ≈105 K, 110 K and 125 K for the 16%, 5.4% and 1.1% filling ratio, respectively, and it decreased down to 80 K after sealing the GGHS. This result can be understood by accounting that, after sealing, the hydrogen gas remaining in the long SS capillary connecting the GGHS to the gas manifold is no longer included in the system. Then, less gas is needed to be absorbed to reach the OFF state and the pressure decreases faster as the sorption pump is cooled. As already mentioned, the OFF state obtained with this sealed switch was characterized on a larger heating power range (Figure 5) and the results are like those obtained by external gas pumping. The thermal characteristic of such sealed device shows that the main goal of this GGHS was fulfilled.

Let us note that this resulting GGHS is not only able to toggle between two distinct conducting states. As a matter of fact, this not so reduced temperature interval of 80 K between these two extreme states can be used to turn this device into a tuneable thermal link able to vary smoothly its thermal conductance by more than two orders of magnitude.

5. Conclusions

Three narrow GGHSs were built and tested in the 150 K to 300 K temperature range. Contrarily to those presented in earlier works, the different parts were joint together by a high temperature silver alloy brazing, which turns these devices more structurally reliable. Using an improved brazing procedure with temperature control to avoid inhomogeneities which may lead to greater

gap lengths, gap length as short as 18 µm at 150 K were obtained in two devices due to the natural difference of the CTE between copper and SS. To obtain the highest possible ON state thermal conductance in this temperature range, the GGHS used hydrogen gas and one of the devices was extensively characterized using this gas where a ON/OFF thermal conductance ratio of 145 was measured. To turn this device compact and autonomous, a hydrogen sorption pump was integrated using the intermetallic $ZrMn_2H_x$ to allow the switching action of the GGHS just by controlling the temperature of the sorption pump filled with this material. By using this alloy, we showed that both ON and OFF states can be obtained within the temperature range of interest (for $T \geq 150$ K). The sealed device, 260 mg of $ZrMn_2$ in the sorption pump, offers a T_{OFF}/T_{ON} temperature of 170 K/250 K. An extended study of this intermetallic material could lead to substantial improvements of the device and would show how tunable are its characteristics. Moreover, beyond $ZrMn_2$, the extensive investigation performed on the materials suitable for H_2 storage should be revisited to build a GGHS working at higher temperatures than that studied in this article, while keeping H_2, the best conducting gas, as the transport medium.

6. References

[1] M. Dietrich, a. Euler, and G. Thummes, "A compact thermal heat switch for cryogenic space applications operating near 100K," *Cryogenics.*, vol. 59, pp. 70–75, Jan. 2014, doi: 10.1016/j.cryogenics.2013.11.004.

[2] S. Vanapalli, R. Keijzer, P. Buitelaar, and H. J. M. ter Brake, "Cryogenic flat-panel gas-gap heat switch," *Cryogenics* ., vol. 78, pp. 83–88, Sep. 2016, doi: 10.1016/j.cryogenics.2016.07.006.

[3] Q. S. Shu, J. A. Demko, and J. E. Fesmire, "Heat switch technology for cryogenic thermal management," *IOP Conf. Ser. Mater. Sci. Eng.*, vol. 278, p. 012133, Dec. 2017, doi: 10.1088/1757-899X/278/1/012133.

[4] M. J. Dipirro and P. J. Shirron, "Heat switches for ADRs," *Cryogenics* ., vol. 62, pp. 172–176, 2014, doi: 10.1016/j.cryogenics.2014.03.017.

[5] J.-M. Duval, P. Camus, M. Calvo, T. Prouvé, O. Exshaw, and D. P. Brasiliano, "Development of an ADR Refrigerator with Two Continuous Stages," *J. Low Temp. Phys.*, vol. 184, no. 3, pp. 604–608, 2016, doi: 10.1007/s10909-016-1568-y.

[6] B. Marland, D. Bugby, and C. Stouffer, "Development and testing of an advanced

cryogenic thermal switch and cryogenic thermal switch test bed," *Cryogenics* ., vol. 44, no. 6–8, pp. 413–420, Jun. 2004, doi: 10.1016/j.cryogenics.2004.03.014.

[7] L. Duband, L. Clerc, E. Ercolani, L. Guillemet, and R. Vallcorba, "Herschel flight models sorption coolers," *Cryogenics* ., vol. 48, no. 3–4, pp. 95–105, Mar. 2008, doi: 10.1016/j.cryogenics.2008.03.016.

[8] G. Bonfait, I. Catarino, J. Afonso, D. Martins, M. Linder, and L. Duband, "20 K Energy storage unit," *Cryogenics* ., vol. 49, no. 7, pp. 326–333, Jul. 2009, doi: 10.1016/j.cryogenics.2009.03.003.

[9] I. Catarino, J. Afonso, D. Martins, M. Linder, L. Duband, and G. Bonfait, "6K solid state Energy Storage Unit," *Cryogenics* ., vol. 50, no. 2, pp. 102–110, Feb. 2010, doi: 10.1016/j.cryogenics.2009.12.002.

[10] I. Catarino, G. Bonfait, and L. Duband, "Neon gas-gap heat switch," *Cryogenics* ., vol. 48, no. 1–2, pp. 17–25, Jan. 2008, doi: 10.1016/j.cryogenics.2007.09.002.

[11] J. Franco, D. Martins, I. Catarino, and G. Bonfait, "Narrow gas gap in cryogenic heat switch," *Appl. Therm. Eng.*, vol. 70, no. 1, pp. 115–121, Sep. 2014, doi: 10.1016/j.applthermaleng.2014.04.062.

[12] J. Franco, B. Galinhas, P. B. de Sousa, D. Martins, I. Catarino, and G. Bonfait, "Building a Thinner Gap in a Gas-Gap Heat Switch," *Phys. Procedia*, vol. 67, pp. 1117–1122, 2015, doi: 10.1016/j.phpro.2015.06.173.

[13] J. Barreto *et al.*, "80 K vibration-free cooler for potential future Earth observation missions," *IOP Conf. Ser. Mater. Sci. Eng.*, vol. 755, p. 012016, Jun. 2020, doi: 10.1088/1757-899X/755/1/012016.

[14] D. Pearson, R. Bowman, M. Prina, and P. Wilson, "The Planck sorption cooler: Using metal hydrides to produce 20K," *J. Alloys Compd.*, vol. 446–447, pp. 718–722, 2007, doi: 10.1016/j.jallcom.2006.11.202.

[15] P. Borges de Sousa, D. Martins, M. Linder, J. Noite, and G. Bonfait, "Liquid-gas hydrogen energy storage unit for the 15–17 K temperature range using an expansion volume at room temperature," *Appl. Therm. Eng.*, vol. 125, pp. 1239–1252, Oct. 2017, doi: 10.1016/j.applthermaleng.2017.06.134.

[16] S. Vanapalli, B. Colijn, C. Vermeer, H. Holland, T. Tirolien, and H. J. M. ter Brake, "A Passive, Adaptive and Autonomous Gas Gap heat Switch," *Phys. Procedia*, vol. 67, pp.

1206–1211, 2015, doi: 10.1016/j.phpro.2015.06.191.

[17] “Cryogenics Material Properties - NIST.” [Online]. Available: https://trc.nist.gov/cryogenics/materials/materialproperties.htm. [Accessed: 09-Sep-2020].

[18] “Online Materials Information Resource - MatWeb,” 2002. [Online]. Available: http://www.matweb.com/. [Accessed: 09-Sep-2020].

[19] Y. S. Touloukian, R. . Kirby, R. E. Taylor, and P. D. Desai, “Volume 12 : Thermal expansion - Metallic Elements and Alloys,” *Thermophys. Prop. Matter-the TPRC Data Ser.*, 1970.

[20] I. Catarino and G. Bonfait, “A simple calorimeter for fast adiabatic heat capacity measurements from 15 to 300 K based on closed cycle cryocooler,” *Cryogenics* ., vol. 40, no. 7, pp. 425–430, 2000, doi: https://doi.org/10.1016/S0011-2275(00)00037-0.

[21] E. W. Lemmon, M. L. Huber, and M. O. Mclinden, “REFPROP 9.1,” *NIST Stand. Ref. database*, 2013.

[22] D. Martins *et al.*, “Sorption characterization and actuation of a gas-gap heat switch,” *Sensors Actuators A Phys.*, vol. 171, no. 2, pp. 324–331, Nov. 2011, doi: 10.1016/j.sna.2011.08.017.

[23] A. O. R. P. Der Nigohossian G., “Adsorption de L’Helium 4 par le Charbon Actif,” *Colloq. Int. du Vide du Froid, Grenoble, Fr.*, p. 22, 1969.

[24] D. Martins, I. Catarino, J. Franco, L. Ribeiro, and G. Bonfait, “Controlled actuation of a Gas-Gap Heat Switch,” in *ICEC 24*, 2012.

[25] G. Morgante *et al.*, “Cryogenic characterization of the Planck sorption cooler system flight model,” *J. Instrum.*, vol. 4, no. 12, pp. T12016–T12016, Dec. 2009, doi: 10.1088/1748-0221/4/12/T12016.

[26] P. Borges de Sousa, D. Martins, M. Linder, J. Noite, and G. Bonfait, “Liquid-gas hydrogen energy storage unit for the 15–17 K temperature range using an expansion volume at room temperature,” *Appl. Therm. Eng.*, vol. 125, pp. 1239–1252, Oct. 2017, doi: 10.1016/j.applthermaleng.2017.06.134.

[27] J. F. Burger, “Cryogenic Microcooling, A micromachined cold stage operating with a sorption compressor in a vapor compression cycle,” Twente University Press (TUP),

Netherlands, 2001.

[28] M. Yoshida and E. Akiba, “Hydrogen absorbing-desorbing properties and crystal structure of the ZrTiNiMnV AB2 Laves phase alloys,” *J. Alloys Compd.*, 1995, doi: 10.1016/0925-8388(95)01518-3.

[29] T. Kodama, “An attempt to estimate the extent of the single phase region of the ZrMn2 phase by means of the X-ray diffraction-profile halfwidths,” *J. Alloys Compd.*, vol. 256, no. 1–2, pp. 263–268, Jul. 1997, doi: 10.1016/S0925-8388(96)03015-0.

[30] P. Bhandari *et al.*, “Sorption Cryocooler Development for the Planck Surveyor Mission,” *Astrophys. Lett. Commun.*, vol. 37, p. 227, 2000.